Azimuthally sensitive femtoscopy in event-by-event hydrodynamics

Piotr Bożek[*]

AGH University of Science and Technology, Faculty of Physics and Applied Computer Science, al. Mickiewicza 30, PL-30059 Krakow, Poland
and The H. Niewodniczański Institute of Nuclear Physics, Polish Academy of Sciences, PL-31342 Kraków, Poland

I analyze the pion femtoscopy correlations in noncentral Au-Au and Pb-Pb collisions. The azimuthally sensitive Hanbury-Brown-Twiss (HBT) method is used to extract the interferometry radii depending on the azimuthal angle with respect to the second- and third-order event plane. The results are in semiquantitative agreement with the STAR collaboration data on the HBT radii with respect to the second-order reaction plane, with the preliminary PHENIX collaboration data on the HBT radii with respect to the third-order reaction plane in Au-Au collisions at 200 GeV, and with the preliminary ALICE collaboration data for the HBT radii with respect to the second-order event plane for Pb-Pb collisions at 2.76 TeV.

I. INTRODUCTION

The collective expansion of the dense fireball in heavy-ion collisions manifests itself as a significant transverse, azimuthally asymmetric flow [1]. The azimuthal asymmetry of the flow originates from the geometrical asymmetry of the participant region in the transverse plane [2] and from event-by-event fluctuations of the fireball shape [3,4].

The size of the emission region can be estimated using femtoscopy methods based on HBT interferometry for identical particles [5]. The HBT radii are extracted from a Gaussian fit to the two-pion correlation function. The radii decrease as a function of the average transverse momentum of the pair, following the change in the size of the homogeneity region [6]. The radii measured at different energies at the Relativistic Heavy Ion Collider (RHIC) [7,8] and the Large Hadron Collider (LHC) [9] indicate a strong correlation between the velocity of the emitting source and its position. The observed correlations are consistent with the existence of a strong collective flow [10].

Azimuthally asymmetric emission geometry and transverse flow lead to angle dependent correlation radii [11–15]. The correlation functions are constructed for pairs of particles in a bin in azimuthal angle. The radii extracted from pairs flying in-plane are different than for pairs flying out-of-plane. The analysis allows one to extract the dependence of the HBT radii on the azimuthal angle. The direction is defined with respect to the event plane. The measured azimuthal dependence of the HBT radii shows a zeroth and second-order harmonic for Au-Au collisions at the AGS [16] and at RHIC [17], Au-Pb collisions at the SPS [18], and Pb-Pb collisions at the LHC [19,20].

The presence of the triangular flow makes it possible to study the azimuthal dependence of the HBT radii with respect to the third-order event plane [21]. The PHENIX collaboration presented preliminary results [22,23] showing a third-order harmonic modulation of the *out* and *side* radii. The theoretical investigation of the relation between the triangular flow and geometry modulations and the observed femtoscopy

radii [24] concludes that the observed HBT radii modulation is determined by the flow. The shape triangularity at freeze-out cannot be directly extracted, unlike the spatial eccentricity.

Azimuthally sensitive femtoscopy radii with respect to the second-order event plane have been extracted from hydrodynamical simulations [25,26]. The results are in fair agreement with experiment. The description of the triangular flow and of the azimuthal dependence of the HBT radii with respect to the third-order event plane requires the application of event-by-event simulations. The analysis of the angle averaged femtoscopy radii in the hydrodynamic model with fluctuating initial conditions indicated a sizable effect of the lumpiness of the emission surface for ideal fluid evolution [27] and a small effect for viscous fluid expansion [28]. Generally, one expects a strong damping of anisotropies through viscous evolution [29]. Angle averaged and azimuthally sensitive HBT radii have been calculated for a range of energies in the ultrarelativistic quantum molecular dynamics model [30,31]. In this paper I present the calculation of the azimuthally sensitive HBT radii for Au-Au collisions at 200 GeV and Pb-Pb collisions at 2.76 TeV within a $3 + 1$ dimensional ($3 + 1$-D) viscous hydrodynamic model [32].

II. MODEL

The expansion of the fireball is described using $3 + 1$-D hydrodynamics [32]. The simulations here presented use a constant shear viscosity to entropy ratio $\eta/s = 0.08$ and bulk viscosity that is nonzero in the hadronic phase $\zeta/s = 0.04$ [33]. The initial density of the fireball is obtained from a Glauber Monte Carlo model [34]. Every event of the Glauber Monte Carlo model constitutes an initial condition for an independent hydrodynamic evolution. The entropy density in the transverse plane is composed from Gaussians of width 0.4 fm at the positions of the participant nucleons; details can be found in [35,36]. The parameters of the model, such as the initial energy density, the contribution of binary collisions, and initial profile in space-time rapidity, are fixed to to reproduce the measured charged particle distribution in pseudorapidity, the transverse momentum spectra ($p_\perp < 2$ GeV), and the elliptic $v_2(p_\perp)$ and triangular $v_3(p_\perp)$ flow of charged particles for
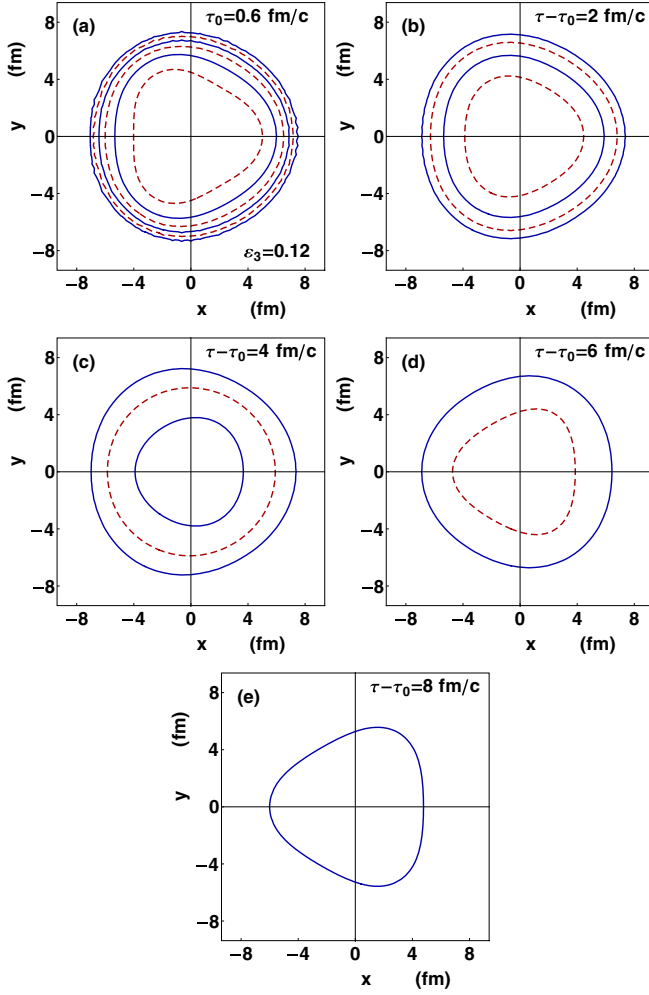
————————
*Piotr.Bozek@ifj.edu.pl

FIG. 1. (Color online) Contours of constant entropy density of the fireball in the transverse plane ($s = 2, 4, 8, 16$ fm$^{-3}, \ldots$). The consecutive panels (a)–(e) show the fireball at different fluid evolution times $\tau_0 = 0.6$ fm/c, $\tau - \tau_0 = 2, 4, 6,$ and 8 fm/c. The initial distribution corresponds to the optical Glauber model density at the impact parameter $b = 0$, with additional triangularity $\varepsilon_3 = 0.12$.
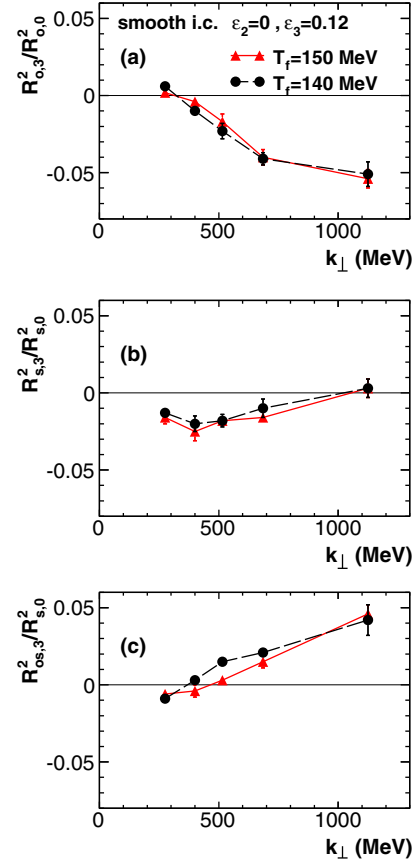

FIG. 2. (Color online) Third-order Fourier coefficient of the azimuthal oscillations of the HBT radii with respect to third-order event plane as function of the transverse momentum for smooth initial conditions [Eq. (2)], $R_{o,3}^2/R_{o,0}^2$ (a), $R_{s,3}^2/R_{s,0}^2$ (b), $R_{os,3}^2/R_{s,0}^2$ (c).

central and semiperipheral Au-Au collisions at 200 GeV and Pb-Pb collisions at 2.76 TeV [36,37]. A satisfactory description of the multiplicity, the average transverse momentum, and the flow asymmetry in the model is necessary in order to study the HBT radii and their momentum and azimuthal angle dependence.

At the freeze-out hypersurface of constant temperature $T_f = 150$ (or 140 MeV when specified) hadrons are emitted statistically. The statistical hadronization and resonance decays are performed using the THERMINATOR code [38]. For each freeze-out hypersurface a large number of real events are generated, by running the THERMINATOR code many times. I take from 100 events for central Pb-Pb collisions at 2.76 TeV up to 1500 events for semiperipheral Au-Au collisions at 200 GeV. The number of independent hydrodynamic runs for each centrality class is 100–400.

The expansion velocity grows faster in the direction of the largest gradient. This stronger flow tends to make the spatial distribution more uniform. Depending on the length of the evolution, the final shape of the fireball may be close to azimuthal symmetry, or in some cases the asymmetry could be inverted with respect to its initial direction. On the other hand, the deformation of the flow,

$$v(r,\phi) = v(r)\{1 + 2a_2 \cos[2(\phi - \psi_2)] \\ + 2a_3 \cos[3(\phi - \psi_3)]\}, \tag{1}$$

is well correlated in its direction ψ_n to the original direction of the elliptic or triangular deformation. The blast-wave models [39] assume some form of the geometry and flow deformation. On the other hand, accurate dynamical simulations can capture different realizations of the flow and geometry deformations at freeze-out. By comparison to the data, this can provide a phenomenological constraint on the degree of final azimuthal asymmetry of the shape.

The change of the azimuthal asymmetry of the fireball in time can be illustrated in a simple example. I take as the initial entropy density the optical Glauber model density $\rho(x,y,b = 0)$ at the impact parameter $b = 0$, for Au-Au collisions at the top RHIC energy. The distribution is modified to introduce a nonzero triangularity,

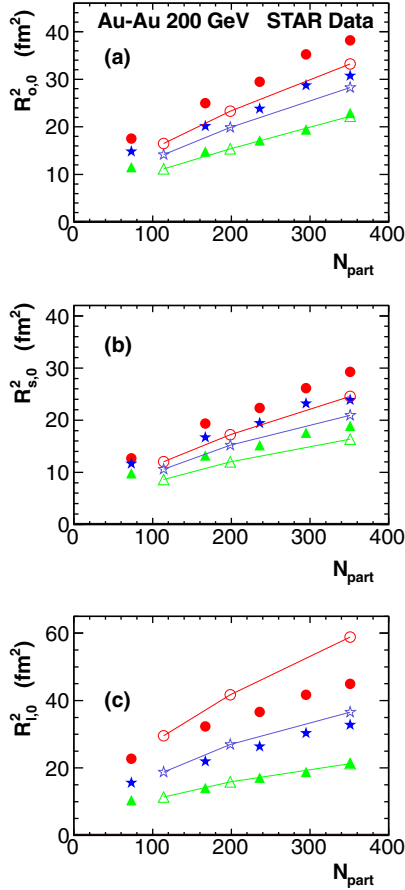$$\rho(x,y) = \rho(x,y,b = 0)e^{e_3 \cos(3\phi)r^2/2\langle r^2\rangle}, \tag{2}$$

FIG. 3. (Color online) HBT radii (zeroth-order Fourier coefficients) with respect to second-order event plane for Au-Au collisions at 200 GeV for different centralities, $R_{o,0}^2$ (a), $R_{s,0}^2$ (b), and $R_{l,0}^2$ (c). STAR collaboration data [17] are denoted by full symbols, circles for 0.15 GeV$< k_\perp < 0.25$ GeV, stars for 0.25 GeV$< k_\perp < 0.35$ GeV, and triangles for 0.35 GeV$< k_\perp < 0.65$ GeV. Results of event-by-event hydrodynamic calculations are shown with open symbols connected with lines.

where $e_3 = 0.3$ and

$$\langle r^2 \rangle = \frac{\int \rho(x,y,b=0)(x^2+y^2)dxdy}{\int \rho(x,y,b=0)dxdy} = 17.5 \text{ fm}^2. \quad (3)$$

The initial triangularity is $\varepsilon_3 = 0.12$.

The transverse expansion is the strongest in the directions $\pm\pi/3$ and π (Fig. 1). After the evolution time of 4 fm/c the geometrical shape is approximately symmetric. Further expansion reverses the deformation [Figs. 1(d) and 1(e)].

III. AZIMUTHALLY SENSITIVE HBT

The symmetrized correlation function of two pions with momenta $p_{1,2}$ emitted at freeze-out from positions $x_{1,2}$ is

$$C(q,k) = \frac{\int d^4x_1 d^4x_2 \langle S(x_1,p_1)S(x_2,p_2)\rangle |\Psi(k,(x_1-x_2))|^2}{\int d^4x_1 \langle S(x_1,p_1)\rangle \int d^4x_2 \langle S(x_2,p_2)\rangle},$$
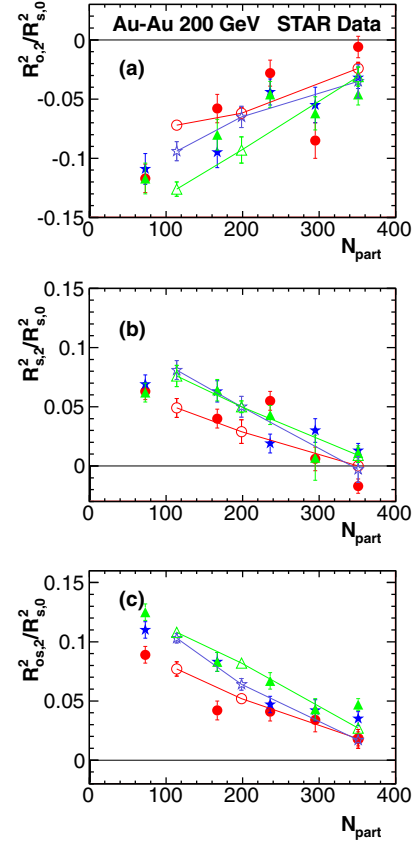
$$(4)$$

FIG. 4. (Color online) Second-order Fourier coefficients of the oscillations of the HBT radii with respect to the second-order event plane for Au-Au collisions at 200 GeV for different centralities, $R_{o,2}^2/R_{s,0}^2$ (a), $R_{s,2}^2/R_{s,0}^2$ (b), $R_{os,2}^2/R_{s,0}^2$ (c). STAR collaboration data [17] are compared to results of hydrodynamic calculations, same symbols as in Fig. 3.

where $q = p_1 - p_2$ is the relative momentum of the pions, $k = (p_1 + p_2)/2$ is the average pair momentum, $\Psi(q,x_1 - x_2) = (e^{iq(x_1-x_2)} + e^{-iq(x_1-x_2)})/\sqrt{2}$ is the two-particle wave function [5]. I neglect final state interactions between the pions. In the experimental analysis Coulomb corrections are applied to the measured correlation functions [40]. In the simulation I assume that the emitted pions do not interact, and no Coulomb corrections are made on the constructed two-particle correlations.

In the experimental analysis, the correlation function is constructed using pairs from the same event in the numerator of Eq. (4) and pairs from mixed events for the denominator. In simulations, due to lower statistics, I combine N_e (100–1600) events corresponding to the same freeze-out hypersurface [28], where each freeze-out surface is generated in a hydrodynamic evolution for a given initial condition. The numerator in correlation function [Eq. (4)] is then averaged over N_h hypersurfaces. This corresponds to the averaging denoted by $\langle \ldots \rangle$. The pairs from mixed events in the denominator are constructed from pions emitted from different freeze-out hypersurfaces. The histogram of the correlation function
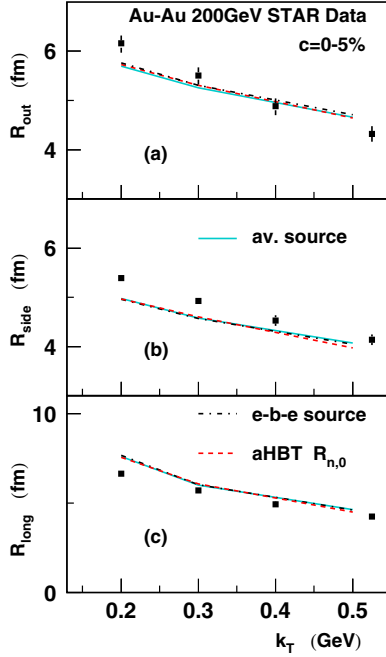
FIG. 5. (Color online) The HBT radii R_o (a), R_s (b), and R_l (c) for Au-Au collisions at 200 GeV; the squares denote the STAR collaboration data [8]. The hydrodynamic model results for event-by-event fluctuating emission sources [Eq. (4)], for the averaged emission source [Eq. (9)], and for the zeroth-order radii from the azimuthally sensitive HBT analysis are represented by the dashed-dotted, solid, and dashed lines respectively.

$C(q,k)$ for a given bin q_a, k_b is

$$C(q_a, k_b)$$
$$= \frac{\frac{1}{N_{\text{pairs,num}}} \sum_{j=1}^{N_h} \sum_{m,l=1}^{N_e} \sum_{s=1}^{M_l} \sum_{f=1}^{M_m} \delta_{q_a} \delta_{k_b} \Psi(q, x_1 - x_2)}{\frac{1}{N_{\text{pairs,den}}} \sum_{i \neq j}^{N_h} \sum_{l,m=1}^{N_e} \sum_{s=1}^{M_l} \sum_{f=1}^{M_m} \delta_{q_a} \delta_{k_b}},$$

$$(5)$$

where M_l and M_m are the pion multiplicities of the events m and l generated from the freeze-out surface j (or i and j in the denominator), the symbols δ_{q_a} and δ_{k_b} are 1 if the momenta $q = p_s - p_f$ and $k = (p_s + p_f)/2$ fall into the respective bins and zero otherwise. The construction of mixed events involves events with different initial conditions, therefore in the denominator the sum runs over pairs of different hydrodynamic simulations ($i \neq j$).

The direction of the second- and third-order event plane ψ is defined as the flow direction taken from N_e combined THERMINATOR events for each hydrodynamically generated freeze-out hypersurface j,

$$v_n e^{in\psi_n^j} = \frac{\sum_{m=1}^{N_e} \sum_{s=1}^{M_m} e^{in\phi_s}}{\sum_{m=1}^{N_e} \sum_{s=1}^{M_m} 1}, \qquad (6)$$

where the sum is taken over the charged particles with pseudorapidity $|\eta| < 2$ (ϕ_s is the azimuthal direction of the particle transverse momentum), $n = 2, 3$ for the second- and third-order event plane respectively. This procedure assures a very good event plane resolution. The azimuthal angles in

the events generated from the hypersurface j are calculated relative to the event plane angle ψ_n^j.

The correlation functions $C(q)$ are calculated in bins in the azimuthal angle Φ and transverse momentum $k_\perp$. The relative momentum is decomposed into q_{long}, q_{out}, and q_{side}, and the correlations function is fitted using the Bertsch-Pratt formula [41,42]. For azimuthally sensitive interferometry at central rapidity and for symmetric collisions I
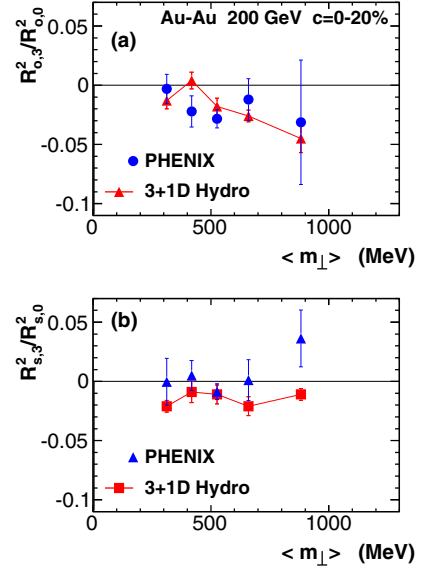

FIG. 6. (Color online) The third-order Fourier coefficients of the oscillations of the HBT radii with respect to third-order event plane for Au-Au collisions at 200 GeV for centrality 0–20% as function of the transverse mass. (a) $R_{o,3}^2/R_{o,0}^2$, preliminary PHENIX data [23] (circles) are compared to hydrodynamic calculations (triangles connected with lines). (b) $R_{s,3}^2/R_{s,0}^2$, preliminary PHENIX data (triangles) are compared to hydrodynamic calculations (squares connected with lines).
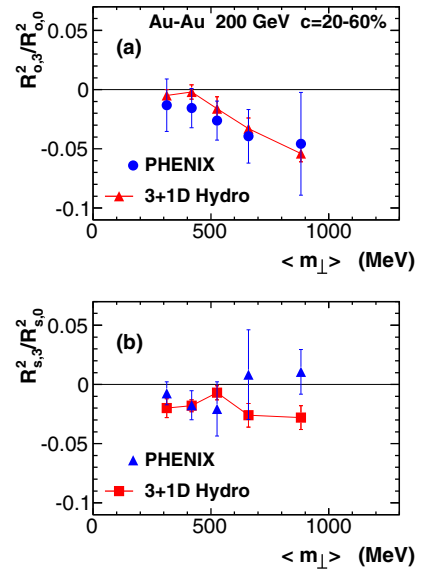

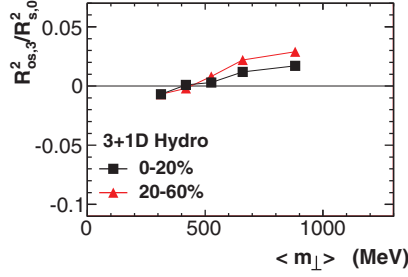FIG. 7. (Color online) Same as Fig. 6 but for centrality 20–60%.

FIG. 8. (Color online) The third-order Fourier coefficients of the oscillations of the HBT radius $R^2_{os,3}/R^2_{s,0}$ with respect to third-order event plane for Au-Au collisions at 200 GeV. Hydrodynamic simulation results for centrality 0–20% and 20–60% are denoted with squares and triangles respectively.

use [12,13]

$$C(q_{\mathrm{long}},q_{\mathrm{out}},q_{\mathrm{side}}) = 1 + \lambda e^{-R^2_o q^2_{\mathrm{out}} - R^2_s q^2_{\mathrm{side}} - R^2_l q^2_{\mathrm{long}} - 2R^2_{os} q_{\mathrm{out}} q_{\mathrm{side}}}. \tag{7}$$

The centrality and $k_\perp$ bins are similar as used in the STAR, PHENIX, and ALICE experiments; I use six bins in the azimuthal direction between 0 and π for the second-order event plane analysis and between 0 and $2\pi/3$ for the third-order event plane analysis. The angular dependence is fitted using the zeroth and second- (third-)order harmonics for the $n = 2$ ($n = 3$) event plane analysis,

$$R^2_o(\Phi) = R^2_{o,0} + 2R^2_{o,n} \cos(n\Phi),$$
$$R^2_s(\Phi) = R^2_{s,0} + 2R^2_{s,n} \cos(n\Phi), \tag{8}$$
$$R^2_{os}(\Phi) = 2R^2_{os,n} \sin(n\Phi).$$

In all cases, the obtained angular dependence of $R_l(\Phi)$ is consistent with a constant value $R_{l,0}$.

I begin with the analysis of the azimuthally sensitive interferometry with respect to the third-order event plane for the fireball with smooth initial conditions described in Sec. II [Eq. (2)]. In that case, there is one hydrodynamic freeze-out surface and Eq. (5) is modified; the sum over the freeze-out hypersurfaces is absent. The scaled third-order HBT radii $R^2_{i,3}$ are shown in Fig. 2. The azimuthal modulation is the largest for the *out* radius $R^2_{o,3}/R^2_{o,0}$. It is negative and its magnitude increases with the transverse momentum. The *side* radius $R^2_{s,3}$ is close to zero and negative. $R^2_{os,3}$ is positive and increases with $k_\perp$. The shape of the geometry of the freeze-out hypersurface is close to azimuthal symmetry for most of the evolution (Fig. 1). The third-order HBT radii are close to the deformed flow scenario [24]. One can notice that the scaled third-order HBT radii do not change substantially when the freeze-out temperature is lowered from 150 to 140 MeV.

The second-order azimuthally sensitive HBT radii for Au-Au collisions at 200 GeV have been analyzed by the STAR collaboration [17]. The ideal fluid hydrodynamic calculation, using smooth initial conditions [26], reproduces semiquantitatively the data. In Figs. 3 and 4 are presented the results of simulations using the event-by-event 3 + 1-D viscous hydrodynamic model. The zeroth-order radii are in semiquantitative
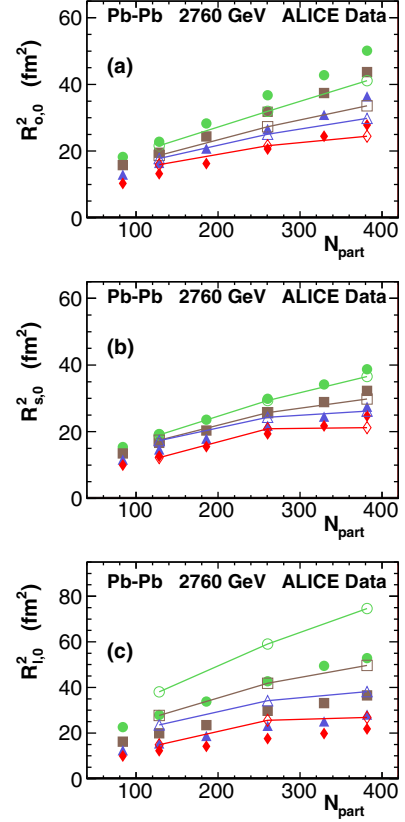

FIG. 9. (Color online) HBT radii (zeroth-order Fourier coefficients) with respect to the second-order event plane for Pb-Pb collisions at 2.76 TeV for different centralities, $R^2_{o,0}$ (a), $R^2_{s,0}$ (b), and $R^2_{l,0}$ (c). Preliminary ALICE collaboration data [20] are denoted by full symbols, circles for 0.2 GeV$< k_\perp < 0.3$ GeV, squares for 0.3 GeV$< k_\perp < 0.4$ GeV, triangles for 0.4 GeV$< k_\perp < 0.5$ GeV, and diamonds for 0.5 GeV$< k_\perp < 0.7$ GeV. Results of event-by-event hydrodynamic calculations are shown with open symbols connected with lines.

agreement with the experimental measurements (Fig. 3). For central collisions (0–5%) the angle averaged HBT radii are the same as the zeroth-order radii $R_{i,0}$ (Fig. 5). The deviations from the data are 10–15%, similar as in other calculations of the angle averaged HBT radii [10]. In Fig. 5 are shown also the results of a calculation using pairs of pions from different hypersurfaces in the numerator of Eq. (5). This corresponds to the use of the event averaged emission function in the numerator of Eq. (4),

$$\begin{aligned} &C_{av}(q,k) \\ &= \frac{\int d^4x_1 d^4x_2 \langle S(x_1,p_1)\rangle \langle S(x_2,p_2)\rangle |\Psi(k,(x_1-x_2))|^2}{\int d^4x_1 \langle S(x_1,p_1)\rangle \int d^4x_2 \langle S(x_2,p_2)\rangle}. \end{aligned} \tag{9}$$

The extracted radii are within 3% from the ones obtained using the correct event-by-event average as in Eq. (4). The second harmonics of the HBT radii are in fair agreement with the experimental results (Fig. 4), both in sign and in magnitude. The second-order components of the radii increase
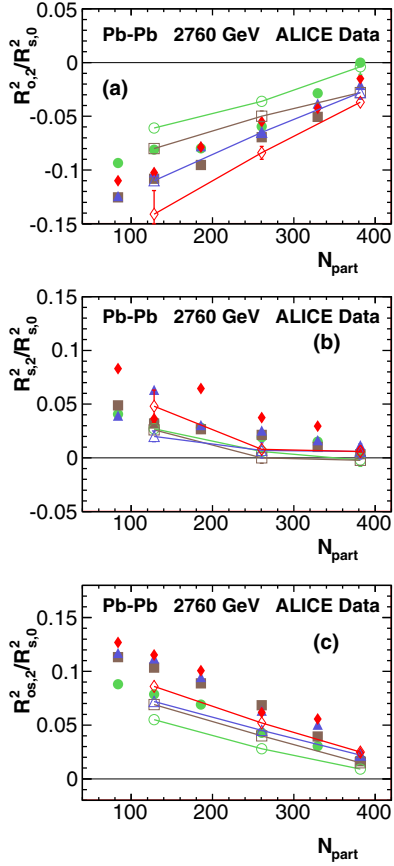
FIG. 10. (Color online) The second-order Fourier coefficients of the oscillations of the HBT radii with respect to second-order event plane for Pb-Pb collisions at 2.76 TeV for different centralities, $R_{o,2}^2/R_{s,0}^2$ (a), $R_{s,2}^2/R_{s,0}^2$ ((b), and $R_{os,2}^2/R_{s,0}^2$ ((c). Preliminary ALICE collaboration data [20] are compared to results of hydrodynamic calculations, same symbols as in Fig. 9.
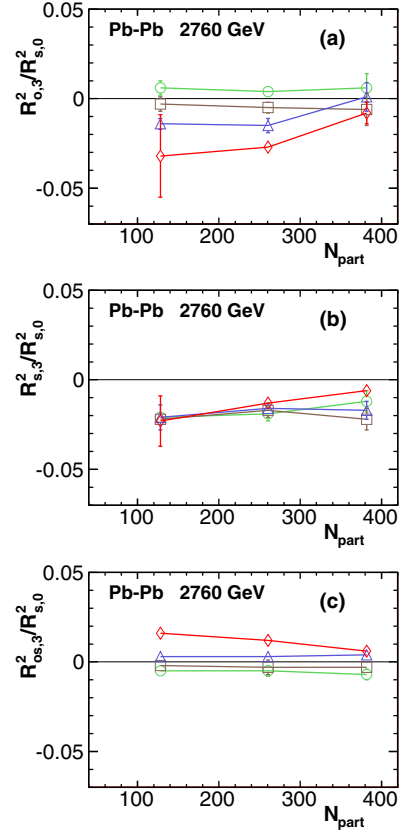

FIG. 11. (Color online) The third-order Fourier coefficients of the oscillations of the HBT radii with respect to third-order event plane for Pb-Pb collisions at 2.76 TeV for different centralities, $R_{o,3}^2/R_{s,0}^2$ (a), $R_{s,3}^2/R_{s,0}^2$ (b), and $R_{os,3}^2/R_{s,0}^2$ (c). Results of hydrodynamic calculations are denoted with the same symbols as in Fig. 9.

with centrality, indicating a stronger deformation of the flow geometry in peripheral events.

The azimuthally sensitive HBT radii with respect to the third-order event plane are calculated for centralities 0–20% and 20–60% and compared to preliminary results of the PHENIX collaboration [20] (Figs. 6 and 7). The scaled radius $R_{o,3}^2/R_{o,0}^2$ is negative and similar as in the experimental data. The agreement is slightly better for the semiperipheral events [Fig. 7(a)]. Its magnitude increases with the transverse mass. The ratio $R_{s,3}^2/R_{s,0}^2$ has a small, negative value. The experimental data points are spread around zero, without a clear systematics of the sign. The third-order harmonic of the $R_{os,3}^2$ radius is positive, increasing with the transverse mass, and larger for the more peripheral events (Fig. 8). One can observe that the results of the realistic, event-by-event calculation for the azimuthally sensitive HBT radii are similar as for the model calculation with smooth initial conditions presented above (Fig. 2). There is no significant centrality dependence of the third-harmonic component of the HBT radii, unlike for the HBT radii with respect to the second-order event plane. This reflects a weaker dependence of the triangular flow on centrality as compared to the elliptic flow.

The azimuthally sensitive HBT radii with respect to the second-order event plane are calculated for Pb-Pb collisions at 2.76 TeV. The zeroth and second-order harmonics are plotted in Figs. 9 and 10. Notice that the calculations are in semiquantitative agreement with the preliminary ALICE collaboration data [20]. The sign of the measured and calculated second harmonics of the HBT radii are similar as for Au-Au collisions at 200 GeV (Fig. 4). The centrality dependence of the second harmonic component of the HBT radii is strong, as expected from the strong centrality dependence of the elliptic flow.

The predictions of the azimuthally sensitive HBT interferometry analysis with respect to the third-order event plane for Pb-Pb collisions are presented in Fig. 11. The results are similar as for Au-Au collisions at RHIC energies. The radii $R_{o,3}^2$ and $R_{s,3}^2$ are negative. The radii $R_{o,3}^2/R_{s,0}^2$ have a larger magnitude, increasing with the transverse momentum and centrality, while $R_{s,3}^2/R_{s,0}^2$ has no noticeable $k_\perp$ dependence. $R_{os,3}^2/R_{s,0}^2$ is positive, increasing with the transverse momentum.

IV. SUMMARY

The azimuthally sensitive interferometry analysis is performed in the event-by-event 3 + 1-D viscous hydrodynamic

model. I construct the two-pion correlation function and calculate the azimuthal dependence of the HBT radii. Two cases are studied, the radii defined with respect to the second- and third-order event planes. For the first case the azimuthal dependence of the radii is decomposed into a zeroth and second harmonic, while in the second case I use the zeroth and third harmonic.

The HBT radii calculated with respect to the second-order event plane are compared to the experimental results of the STAR and ALICE collaborations for Au-Au collisions at 200 GeV [17] and Pb-Pb collisions at 2.76 TeV [20]. The sign and the magnitude of the calculated second-order harmonics of the HBT radii is in semiquantitative agreement with the experimental results. I find a strong centrality dependence of the scaled ratios $R_{o,2}^2/R_{s,0}^2$, $R_{s,2}^2/R_{s,0}^2$, and $R_{os,2}^2/R_{s,0}^2$.

The third harmonic of the azimuthal dependence of the HBT radii with respect to the third-order event plane is calculated for RHIC and LHC energies. AT RHIC energies, I find a negative value of $R_{o,3}^2/R_{o,0}^2$, with a magnitude increasing with the

transverse momentum, and with weak centrality dependence. These effects are in agreement with preliminary PHENIX collaboration data [23]. The calculated $R_{s,3}^2/R_{s,0}^2$ is small and negative, with no significant dependence on transverse momentum. The predicted value of $R_{os,3}^2/R_{s,0}^2$ is positive and increases with the transverse momentum. The predictions for the third-order HBT radii in Pb-Pb collisions at 2.76 TeV are qualitatively similar.

During the dynamic expansion of the fireball the initial triangular deformation is washed out, or even reversed. The model gives large magnitude, negative values of $R_{o,3}^2$ and small magnitude, negative values of $R_{s,3}^2$. Detailed experimental and model studies may serve as a way to establish the size and the sign of the triangular deformation at freeze-out.

[1] W. Florkowski, *Phenomenology of Ultra-Relativistic Heavy-Ion Collisions* (World Scientific, Singapore, 2010); U. Heinz and R. Snellings, Annu. Rev. Nucl. Part. Sci. **63**, 123 (2013); C. Gale, S. Jeon, and B. Schenke, Int. J. Mod. Phys. A **28**, 1340011 (2013); M. Luzum and H. Petersen, arXiv:1312.5503.

[2] J. Y. Ollitrault, Phys. Rev. D **46**, 229 (1992).

[3] B. Alver *et al.* (PHOBOS Collaboration), Phys. Rev. Lett. **98**, 242302 (2007).

[4] B. Alver and G. Roland, Phys. Rev. C **81**, 054905 (2010); H. Petersen, G.-Y. Qin, S. A. Bass, and B. Muller, *ibid.* **82**, 041901 (2010); B. H. Alver, C. Gombeaud, M. Luzum, and J.-Y. Ollitrault, *ibid.* **82**, 034913 (2010).

[5] U. A. Wiedemann and U. W. Heinz, Phys. Rep. **319**, 145 (1999); U. W. Heinz and B. V. Jacak, Annu. Rev. Nucl. Part. Sci. **49**, 529 (1999); M. A. Lisa, S. Pratt, R. Soltz, and U. Wiedemann, *ibid.* **55**, 357 (2005); M. Lisa, E. Frodermann, G. Graef, M. Mitrovski, E. Mount *et al.*, New J. Phys. **13**, 065006 (2011).

[6] S. Akkelin and Y. Sinyukov, Phys. Lett. B **356**, 525 (1995).

[7] B. Abelev *et al.* (STAR Collaboration), Phys. Rev. C **80**, 024905 (2009).

[8] J. Adams *et al.* (STAR Collaboration), Phys. Rev. C **71**, 044906 (2005).

[9] K. Aamodt *et al.* (ALICE Collaboration), Phys. Lett. B **696**, 328 (2011).

[10] W. Broniowski, M. Chojnacki, W. Florkowski, and A. Kisiel, Phys. Rev. Lett. **101**, 022301 (2008); S. Pratt, *ibid.* **102**, 232301 (2009); P. Bożek, Phys. Rev. C **83**, 044910 (2011); I. A. Karpenko, Y. M. Sinyukov, and K. Werner, *ibid.* **87**, 024914 (2013).

[11] S. A. Voloshin and W. E. Cleland, Phys. Rev. C **53**, 896 (1996).

[12] U. A. Wiedemann, Phys. Rev. C **57**, 266 (1998).

[13] M. A. Lisa, U. W. Heinz, and U. A. Wiedemann, Phys. Lett. B **489**, 287 (2000).

[14] U. W. Heinz and P. F. Kolb, Phys. Lett. B **542**, 216 (2002).

[15] U. Heinz, A. Hummel, M. A. Lisa, and U. A. Wiedemann, Phys. Rev. C **66**, 044903 (2002).

[16] M. Lisa *et al.* (E895 Collaboration), Phys. Lett. B **496**, 1 (2000).

[17] J. Adams *et al.* (STAR Collaboration), Phys. Rev. Lett. **93**, 012301 (2004).

[18] D. Adamova *et al.* (CERES Collaboration), Phys. Rev. C **78**, 064901 (2008).

[19] J. Gramling, Diploma Thesis, University of Heidelberg, 2011, CERN-THESIS-2012-088.

[20] V. Loggins (ALICE Collaboration), talk given at the Workshop on Correlations and Femtoscopy, Acireale, Nov. 5–8, 2013.

[21] S. A. Voloshin, J. Phys. G **38**, 124097 (2011).

[22] T. Niida (PHENIX Collaboration), Nucl. Phys. A **904-905**, 439c (2013).

[23] T. Niida (PHENIX Collaboration), talk given at the Workshop on Correlations and Femtoscopy, Acireale, Nov. 5–8, 2013.

[24] C. J. Plumberg, C. Shen, and U. W. Heinz, Phys. Rev. C **88**, 044914 (2013).

[25] E. Frodermann, R. Chatterjee, and U. Heinz, J. Phys. G **34**, 2249 (2007).

[26] A. Kisiel, W. Broniowski, M. Chojnacki, and W. Florkowski, Phys. Rev. C **79**, 014902 (2009).

[27] O. Socolowski, F. Grassi, Y. Hama, and T. Kodama, Phys. Rev. Lett. **93**, 182301 (2004).

[28] P. Bożek, Phys. Lett. B **717**, 287 (2012).

[29] B. Schenke, S. Jeon, and C. Gale, Phys. Rev. Lett. **106**, 042301 (2011).

[30] Q. Li, G. Graf, and M. Bleicher, Phys. Rev. C **85**, 034908 (2012).

[31] G. Graef, M. Bleicher, and M. Lisa, Phys. Rev. C **89**, 014903 (2014).

[32] P. Bożek, Phys. Rev. C **85**, 034901 (2012).

[33] P. Bożek, Phys. Rev. C **81**, 034909 (2010).

[34] M. Rybczynski, G. Stefanek, W. Broniowski, and P. Bozek, arXiv:1310.5475.

[35] P. Bożek, Phys. Rev. C **85**, 014911 (2012).

[36] P. Bożek and W. Broniowski, Phys. Rev. C **85**, 044910 (2012).

[37] P. Bożek and I. Wyskiel-Piekarska, Phys. Rev. C **85**, 064915 (2012).

[38] M. Chojnacki, A. Kisiel, W. Florkowski, and W. Broniowski, Comput. Phys. Commun. **183**, 746 (2012).

[39] F. Retiere and M. A. Lisa, Phys. Rev. C **70**, 044907 (2004).

[40] M. G. Bowler, Phys. Lett. B **270**, 69 (1991); Y. Sinyukov, R. Lednicky, S. V. Akkelin, J. Pluta, and B. Erazmus, *ibid.* **432**, 248 (1998).

[41] G. F. Bertsch, Nucl. Phys. A **498**, 173 (1989).

[42] S. Pratt, Phys. Rev. D **33**, 1314 (1986).